Supplementary material

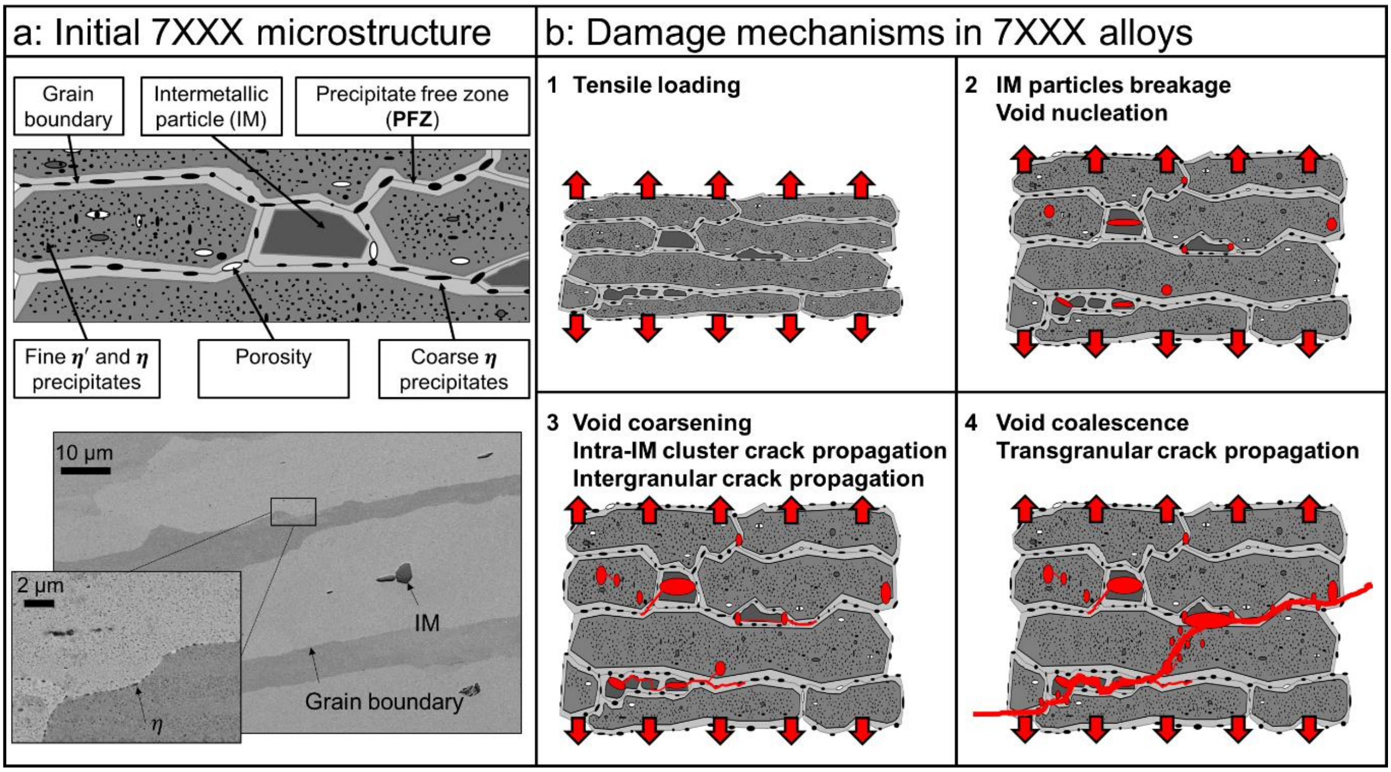

Figure S1: a) Typical schematized 7XXX microstructure and actual microstructure of 7475 rolled material. b) Damage mechanisms in 7XXX alloys under uniaxial loading, schematized steps leading to failure: 1 loading, 2 damage nucleation, 3 damage coarsening, 4 final crack propagation.

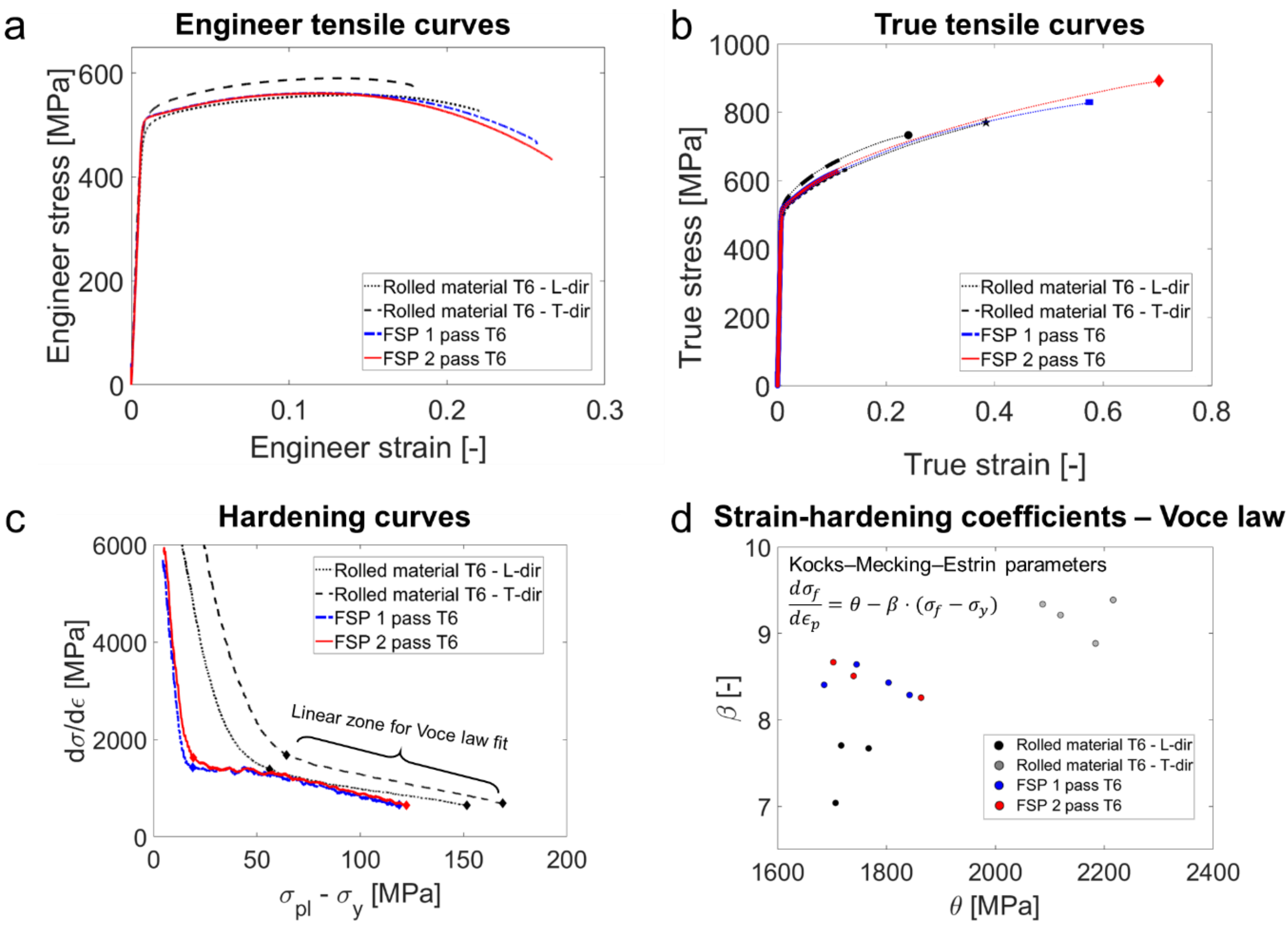

Figure S2: a) Engineering tensile curves of T6 7475 alloy either rolled or FSPed 1 or 2 pass. b) True stress-strain curves in plain line, post-mortem measurement of true fracture strain displayed and linked with dashed thin lines with the tensile measurements. c) Hardening curves of studied microstructures, from yield initiation to ultimate tensile stress. An elasto-plastic transition precedes the flat stage used for Voce law fitting. d) Hardening parameters following the Voce law. Measurements are based on the linear part of the curves of Figure S2c, in between diamond symbols. θ stands for dislocation storage rate – β for the recovery rate. See [Simar et al. MSEA 486, 2008] for a detailed procedure.

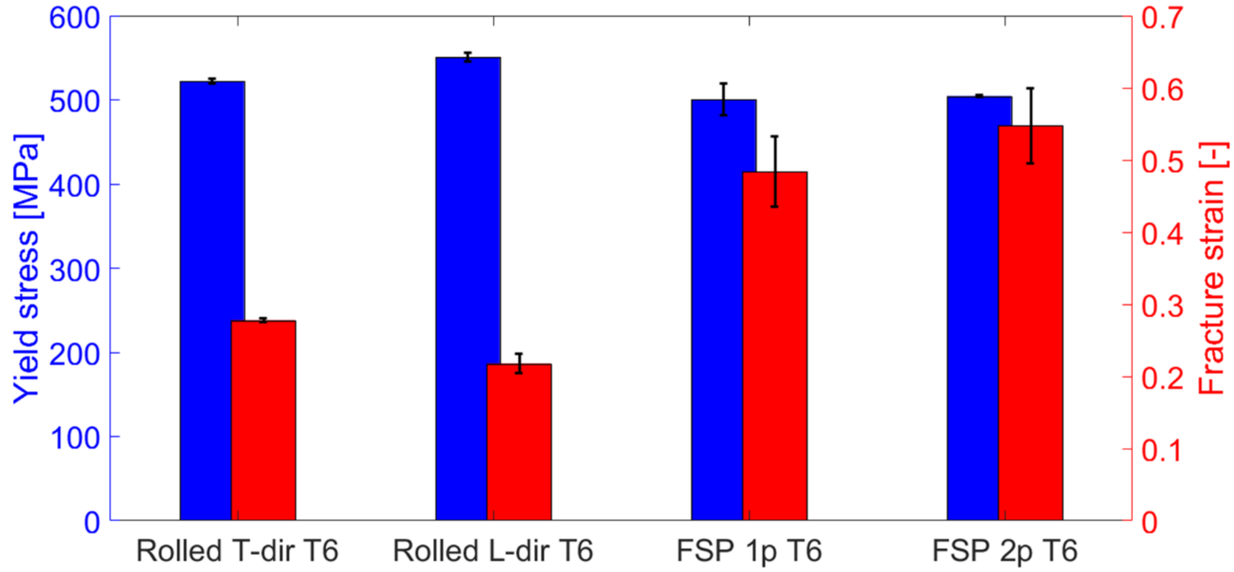

Figure S3: Yield strength and ductility of rolled T6 7475 alloy and after 1 and 2 pass FSP + T6 heat treatment, similarly to 7475 alloy (Figure 3 main paper). FSP increases the fracture strain without affecting the yield strength. The second FSP pass further enhances this ductility improvement.

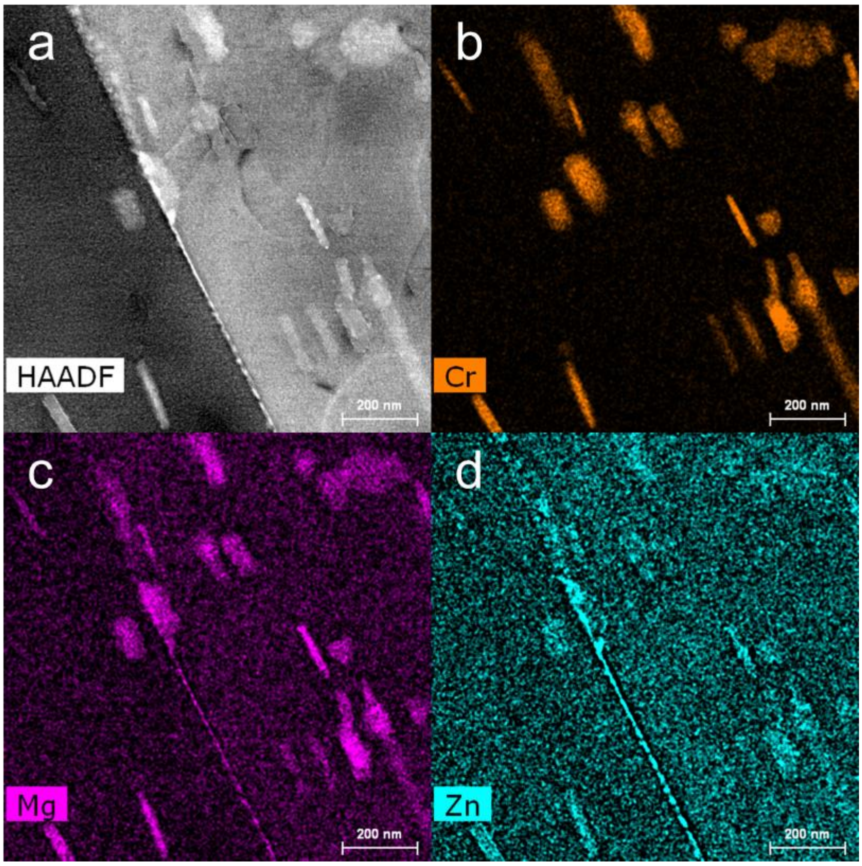

Figure S4: HAADF-STEM image (a) and corresponding EDX maps of Cr (b), Mg (c) and Zn (d). The coarser Cr-rich dispersoids are located inside the rolled T6 material (b) while the coarse $MgZn_2$ η precipitates inside PFZ are identified at the grain boundary (c-d).